UC Irvine
UC Irvine Previously Published Works

Title
Observations of C1–C5 alkyl nitrates in the Yellow River Delta, northern China: Effects of biomass burning and oil field emissions

Permalink
https://escholarship.org/uc/item/3f10z3d2

Authors
Zhang, Yingnan
Sun, Jingjing
Zheng, Penggang
et al.

Publication Date
2019-03-01

DOI
10.1016/j.scitotenv.2018.11.208

Peer reviewed

Observations of C_1–C_5 alkyl nitrates in the Yellow River Delta, northern China: Effects of biomass burning and oil field emissions

Yingnan Zhang [a], Jingjing Sun [a], Penggang Zheng [a], Tianshu Chen [a], Yuhong Liu [a], Guangxuan Han [b], Isobel J. Simpson [c], Xinfeng Wang [a], Donald R. Blake [c], Zeyuan Li [a], Xue Yang [a], Yanbin Qi [d,e], Qi Wang [d,e], Wenxing Wang [a], Likun Xue [a,f,*]

[a] Environment Research Institute, Shandong University, Ji'nan, Shandong, China
[b] Key Laboratory of Coastal Environmental Process and Ecology Remediation, Yantai Institute of Coastal Zone Research, Chinese Academy of Sciences, Yantai, Shandong, China
[c] Department of Chemistry, University of California at Irvine, Irvine, CA, United States
[d] Jilin Weather Modification Office, Changchun, Jilin, China
[e] Joint Laboratory of Weather Modification for Chinese Meteorological Administration and People's Government of Jilin Province (Key Laboratory of Jilin Province), Changchun, Jilin, China
[f] Ji'nan Institute of Environmental Science, Ji'nan, Shandong, China

HIGHLIGHTS

- The tempo-spatial variations of C_1-C_5 alkyl nitrates and parent hydrocarbons were examined in the Yellow River Delta.
- Oil field emissions and biomass burning are important sources of hydrocarbons and alkyl nitrates in this region.
- Besides parent hydrocarbons, longer alkanes are important precursors of alkyl nitrates in oil fields.

GRAPHICAL ABSTRACT
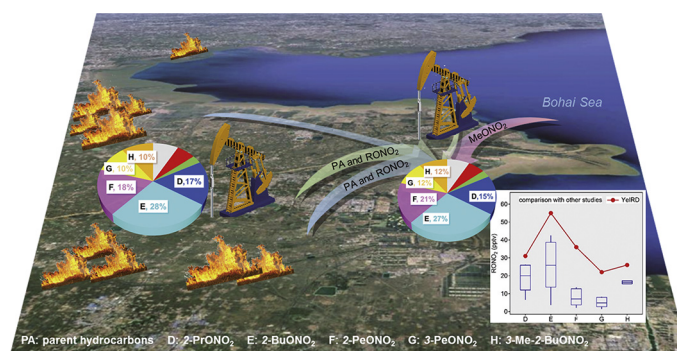
ARTICLE INFO

ABSTRACT

Alkyl nitrates ($RONO_2$) are important reservoirs of nitrogen oxides and play key roles in the tropospheric chemistry. Two phases of intensive campaigns were conducted during February–April and June–July of 2017 at a rural coastal site and in open oil fields of the Yellow River Delta region, northern China. C_1–C_5 alkyl nitrates showed higher concentration levels in summer than in winter-spring ($p < 0.01$), whilst their parent hydrocarbons showed an opposite seasonal variation pattern. The C_3–C_5 $RONO_2$ levels in the oil fields were significantly higher than those in the ambient rural air. Alkyl nitrates showed well-defined diurnal variations, elucidating the effects of in-situ photochemical production and regional transport of aged polluted plumes. Backward trajectory analysis and fire maps revealed the significant contribution of biomass burning to the observed alkyl nitrates and hydrocarbons. A simplified sequential reaction model and an observation-based chemical box model were deployed to diagnose the formation mechanisms of C_1–C_5 $RONO_2$. The C_3–C_5 $RONO_2$ were mainly produced from the photochemical oxidation of their parent hydrocarbons (i.e., C_3–C_5 alkanes), whilst C_1–C_2 $RONO_2$ compounds have additional sources. In addition to parent hydrocarbons, longer alkanes with >4 carbon atoms were also important precursors of alkyl nitrates in the oil fields. This study demonstrates the significant effects

* Corresponding author at: Environment Research Institute, Shandong University, Ji'nan, Shandong, China.
  E-mail address: xuelikun@sdu.edu.cn (L. Xue).

Sequential reaction model
Yellow River Delta

of oil field emissions and biomass burning on the volatile organic compounds and alkyl nitrate formation, and provides scientific support for the formulation of control strategies against photochemical air pollution in the Yellow River Delta region.

1. Introduction

Alkyl nitrates ($RONO_2$) are an important family member of the reactive odd nitrogen ($NO_y = NO + NO_2 + NO_3 + N_2O_5 + HONO + HNO_3 + NO_3^- + PANs + RONO_2 + $ etc.), which are crucial players of atmospheric chemistry and have significant consequences to regional air quality, ecosystem, and climate change (Jenkin and Clemitshaw, 2000). They have relatively low chemical reactivity, and can release NO_2 via photolysis (Atkinson et al., 2006; Sommariva et al., 2008). Due to this nature, alkyl nitrates can serve as temporary reservoirs of nitrogen oxides ($NO_x = NO + NO_2$) during long-range transport, redistribute NO_x between urban and rural (or remote) areas, and hence affect the regional and even global ozone (O_3) formation (Day et al., 2003). Thus, investigation of characteristics and sources of alkyl nitrates is an important step towards better understanding of the formation of regional photochemical pollution.

In the troposphere, alkyl nitrates are mainly formed through photochemical degradation of volatile organic compounds (VOCs) in the presence of NO_x (Arey et al., 2001; Atkinson et al., 2006). Briefly, oxidation of hydrocarbons by the hydroxyl radical (OH) produces a RO_2 radical, which can then react with NO to yield $RONO_2$ (Arey et al., 2001). For each $RONO_2$ species, there are only a small number of precursor hydrocarbons, the degradation of which can exactly yield the specific RO_2 radical (e.g., CH_3O_2 for methyl nitrate, $C_2H_5O_2$ for ethyl nitrate, etc.). In general, the longer and more complex is the chain of the RO_2 radical, the fewer are the precursor hydrocarbons of the $RONO_2$ species. For instance, the formation of the longer-chain (e.g., $\geq C_3$) $RONO_2$ is usually dominated by the oxidation of parent alkanes (e.g., propane for $PrONO_2$, butane for $BuONO_2$, pentane for $PeONO_2$, etc.), whilst C_1–C_2 $RONO_2$ can be formed from the other VOCs that can decompose to CH_3O_2 and $C_2H_5O_2$ radicals, in addition to their parent alkanes (i.e., methane and ethane) (Russo et al., 2010; Sun et al., 2018). Besides, ambient alkyl nitrates are also subject to primary emissions in specific circumstances. In coastal areas, for example, marine emissions are an important source of shorter-chain $RONO_2$, especially methyl nitrate (Atlas et al., 1993; Blake et al., 2003; Song et al., 2018). Biomass burning has been also recognized as a significant source contributing to the ambient $RONO_2$ (Simpson et al., 2002). Identification of the principal sources and secondary formation mechanisms is fundamental to formulating the control strategies against alkyl nitrate pollution in a specific region.

In recent decades, photochemical air pollution characterized by high concentrations of O_3 and other secondary pollutants (such as PANs and $RONO_2$, etc.) has become a major environmental concern in China, as a result of its fast urbanization process (Wang et al., 2006; Wang et al., 2017; Xue et al., 2014a). A number of field studies have been carried out to evaluate the characteristics and formation mechanisms of O_3 pollution in the fast developing regions of China, such as the Jing-Jin-Ji region, Pearl River Delta, and Yangtze River Delta (Wang et al., 2017; and references therein), whilst relatively limited efforts have focused on alkyl nitrates (Ling et al., 2016; Lyu et al., 2015; Sun et al., 2018; Wang et al., 2013). The Yellow River Delta region (YelRD) is located in the mouth of the Yellow River in Shandong province, and lies in between the Shandong Peninsula and Beijing-Tianjin area (see Fig. 1). With a population of 10 million, it is home to the second largest oil field (Shengli Oil Field) in China with numerous refinery and petrochemical plants, and now is one of the most economically dynamic regions in China. It is also an important agricultural area and a coastal wetland in northern China. Given the above features, it can be expected that the YelRD region should be suffering from serious air pollution problems, especially photochemical pollution. To the best of our knowledge, however, there have been no previous studies to investigate the photochemical pollution in this region and evaluate the impacts of the oil extraction and petrochemical industries.

To investigate the photochemical air pollution and its formation mechanisms in the YelRD region, intensive field campaigns were
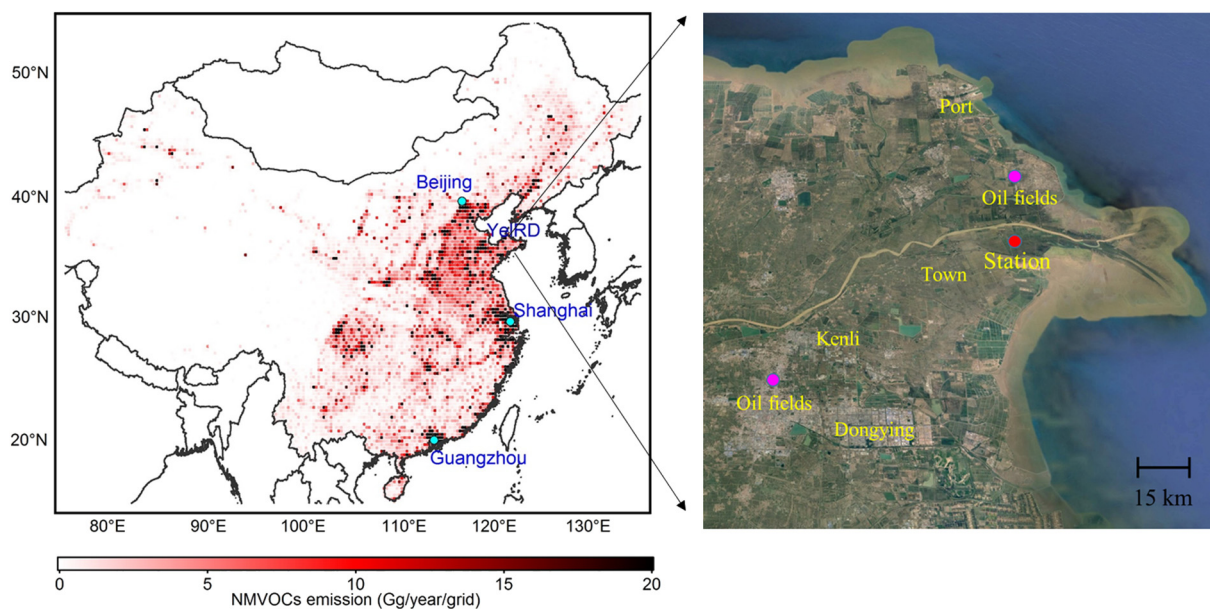

Fig. 1. Maps showing the Yellow River Delta region (YelRD) as well as the locations of the study site and oil field samples. The emission data of non-methane VOCs were taken from Li et al. (2017).

conducted at a rural site surrounded by oil fields and directly in the open oil fields during selected months of 2017. A large suite of air pollutants and meteorological parameters were measured in-situ. This paper analyzes the tempo-spatial variations, sources, and secondary formation regimes of $C_1–C_5$ $RONO_2$ in the YelRD region. Elevated concentrations of alkyl nitrates were observed in the oil fields, where longer chain alkanes are important $RONO_2$ precursors besides the well-known short chain parent hydrocarbons. Oil field emissions and biomass burning are major sources of alkyl nitrates and photochemical air pollution in the region. Overall, this study provides some new insights into the characterization and sources of alkyl nitrates in the oil-extracting areas, and can support the formulation of control strategies against photochemical pollution in the YelRD region.

2. Methodology

2.1. Site description

The sampling campaigns were conducted at the Yellow River Delta Ecology Research Station of Coastal Wetland (37°45′N, 118°58′E; 0 m above sea level), Chinese Academy of Sciences. It is a typical rural coastal site located at the mouth of the Yellow River with few local anthropogenic emissions (see Fig. 1). The closest populated area around our site is a small town with a population of 25,000, 16 km to the southwest. The major nearby urban areas are Dongying city (with 2.1 million population) and Kenli District (248,200 population), which are situated approximately 50 and 40 km to the southwest of the station, respectively. Several open oil fields and a number of petrochemical plants are located to the north and southwest of the station with average distances >15 and 45 km, respectively. In addition, a port with a transport capacity of 50 million tons per year is located about 36 km to the north. Two phases of sampling campaigns were carried out from 8 February to 1 April and from 1 June to 10 July 2017, respectively. To better understand the impacts of oil field emissions on VOCs and alkyl nitrate formation, a dozen whole air samples were collected directly in the open oil fields (see Fig. 1) on selected days (i.e., 5 March and 3 April in winter-spring, 26 June and 9 July in summer).

2.2. Measurement techniques

Whole air samples were collected in 2 Liter stainless-steel canisters, which were cleaned and evacuated prior to the sampling. The sampling days were carefully selected according to the air quality forecast provided by the Ministry of Ecology and Environment of China. On pollution episode days, six samples were collected, each over a 3-min period, with a 3-h interval from 6:00–21:00 (local time (LT)) during the winter-spring phase (on 19, 22, 23, 27 and 28 February and 11, 23 and 29 March 2017) and at a 2-h interval from 8:00–18:00 (LT) in summer (on 8, 9, 14, 15, 16, 18, 29 and 30 June and 3, 9 July 2017). During the non-episode days, sampling was made once typically at 12:00 (LT). Totally 133 samples were taken including 64 and 69 samples in the two phases, respectively. After the sampling, the canisters were immediately sent to the University of California at Irvine for chemical analyses. Detailed information on the analytical procedures, detection limit, and measurement precision can be found elsewhere (Colman et al., 2001; Simpson et al., 2006). Concisely, eight $C_1–C_5$ $RONO_2$ compounds, i.e., methyl nitrate ($MeONO_2$), ethyl nitrate ($EtONO_2$), 1-propyl nitrate (1-$PrONO_2$), 2-propyl nitrate (2-$PrONO_2$), 2-butyl nitrate (2-$BuONO_2$), 2-pentyl nitrate (2-$PeONO_2$), 3-pentyl nitrate (3-$PeONO_2$) and 3-methyl 2-butyl nitrate (3-Me-2-$BuONO_2$), together with 75 $C_1–C_{10}$ hydrocarbons were detected using multi-column gas chromatography (GC) coupled with electron capture detection (ECD), flame ionization detection (FID), and mass spectrometer detection (MSD). The detection limit of the $RONO_2$ measurements was sub-pptv and the measurement precision was 5%. The VOC detection limit was 3 pptv and the typical measurement precision was 3%.

Table 1
Detailed information of instrument techniques used in the present study.

Species	Instrument techniques	Detection limit (ppbv)	Precision
O_3	T-API[a], model T400	0.4	0.5%
NO & NO_y	T-API[a], model T200U	0.05	0.5%
NO_2	T-API[a], model T500U	0.04	0.5%
CO	T-API[a], T300U	20	0.5%
SO_2	TEI[b], model 43C	1	1%
HONO	QUMA, model LOPAP-03	0.003	1%

[a] T-API: Teledyne Advanced Pollution Instrumentation.
[b] TEI: Thermo Electron Instruments.

Real-time measurements of related traces gases and meteorological parameters were also carried out. The detailed information of the instrument techniques and their corresponding detection limit and precision is summarized in Table 1. Here we only give a brief introduction. O_3 was measured by a UV photometric ozone analyzer. NO and NO_y were monitored using a chemiluminescence analyzer, with NO_y being converted to NO by an externally-placed molybdenum oxide converter prior to detection. NO_2 was monitored by an optical analyzer. CO was measured by a gas filter correlation, non-dispersive infrared analyzer. SO_2 was monitored by a pulsed fluorescence gas analyzer. HONO was measured using a long path absorption photometer (Li et al., 2018). Meteorological parameters including temperature, relative humidity, wind vectors, and solar radiation were recorded by a set of commercial meteorological sensors within an Automatic Meteorological Station. Details about the quality assurance and quality control procedures have been documented elsewhere (Li et al., 2018; Sun et al., 2018; Xue et al., 2011).

2.3. Sequential reaction model

In this study, the photochemical evolution of alkyl nitrates and their parent hydrocarbons was examined using a simplified sequential reaction model, which was developed by Bertman et al. (1995) and subsequently has been applied in many previous studies (Reeves et al., 2007; Russo et al., 2010; Sun et al., 2018; Worton et al., 2010). Briefly, this sequential reaction model considers the OH oxidation of parent hydrocarbons as well as formation and loss of alkyl nitrates, including the rate constants and branching ratios of related reactions. Then, the relationship between alkyl nitrates and their parent hydrocarbons can be expressed as a function of reaction time (t) according to the following equations:

$$\frac{RONO_2}{RH} = \frac{\beta k_A}{k_B - k_A}\left(1 - e^{(k_A - k_B)t}\right) + \frac{[RONO_2]_0}{[RH]_0}e^{(k_A - k_B)t} \tag{E1}$$

$$k_A = k_1 \times [OH] \tag{E2}$$

$$k_B = k_2 \times [OH] + J_{RONO_2} \tag{E3}$$

$$\beta = \alpha_1\alpha_2 \tag{E4}$$

Table 2
The branching ratios leading to the formation of alkyl nitrates from oxidation of parent hydrocarbons.
These values are obtained from Kwok and Atkinson (1995), Simpson et al. (2003) and Wang et al. (2013).

Alkyl nitrate ($RONO_2$)	Parent alkane (RH)	Branching ratios		
		α_1	α_2	β
$MeONO_2$	Methane	1	0.001	0.001
$EtONO_2$	Ethane	1	0.006	0.006
1-$PrONO_2$	Propane	0.264	0.02	0.006
2-$PrONO_2$	Propane	0.736	0. 042	0.029
2-$BuONO_2$	n-Butane	0.873	0.09	0.077
2-$PeONO_2$	n-Pentane	0.55	0.13	0.072
3-$PeONO_2$	n-Pentane	0.35	0.13	0.046

Table 3
Descriptive statistics of C_1–C_5 $RONO_2$ and their parent hydrocarbons observed over the Yellow River Delta region during the sampling campaigns (units: pptv unless otherwise specified).

Species	Summer						Winter-spring					
	Rural air			Oil fields			Rural air			Oil fields		
	Mean	SD	Median	Mean	SD	Median	Mean	SD	Median	Mean	SD	Median
$MeONO_2$	15.3	4.1	15.6	13.7	6.0	12.3	11.9	3.4	11.4	11.8	6.0	10.8
$EtONO_2$	12.6	3.9	12.9	10.4	3.1	9.6	7.8	2.5	7.3	9.1	4.5	6.4
$1\text{-}PrONO_2$	5.7	2.0	5.8	5.1	2.0	4.8	4.5	1.8	4.3	5.0	3.0	3.3
$2\text{-}PrONO_2$	30.8	11.8	30.4	32.9	16.6	29.1	25.5	8.9	24.0	28.6	16.8	19.1
$2\text{-}BuONO_2$	55.2	27.2	52.9	62.2	36.3	55.9	38.7	16.5	35.8	50.3	36.3	29.4
$2\text{-}PeONO_2$	36.4	21.7	30.9	51.2	31.9	41.8	22.9	11.6	19.9	32.2	26.7	16.8
$3\text{-}PeONO_2$	21.6	12.1	20.1	29.1	17.9	25.0	13.4	6.3	11.9	21.1	16.7	11.5
$3\text{-}Me\text{-}2\text{-}BuONO_2$	26.4	14.4	23.9	35.1	19.2	33.4	8.3	4.2	7.3	10.8	9.7	4.8
Methane (ppbv) (ppbv)	2184	146	2184	2754	1012	2433	2116	159	2089	8043	6829	5333
Ethane	3543	1392	3129	32,785	34,726	13,368	5786	2275	6091	73,007	62,292	75,456
Propane	3560	2054	3353	48,027	53,338	18,312	4940	3281	5380	77,854	50,357	89,776
n-Butane	2121	1388	2231	30,421	39,523	16,699	2559	2336	2546	22,719	25,220	8317
n-Pentane	738	543	781	16,959	18,866	8460	965	913	909	9102	8691	6470
i-Pentane	1037	712	1042	12,807	16,646	9477	1345	1202	1361	11,527	10,183	7052
T (°C)	25.9	4.5	26.1	–	–	–	3.6	5.2	2.7	–	–	–
RH (%)	76	16	82	–	–	–	71	18	75	–	–	–

where RH refers to the parent hydrocarbons of alkyl nitrates; $[RONO_2]_0/[RH]_0$ is the initial ratio of $RONO_2/RH$, and was calculated as the observed lowest ratios in each campaign. Based on the MCM model simulations, daytime average [OH] concentrations of 2×10^6 and 1×10^6 molecule cm^{-3} were adopted in this study for summer and winter-spring campaigns, respectively. Among these parameters, α_1 and α_2 are the branching ratios of RH + OH and RO_2 + NO reactions leading to $RONO_2$ formation, and their values are summarized in Table 2. k_A and k_B represent the pseudo-first-order rate constants for alkyl nitrate production and removal, respectively. And k_1 and k_2 are the rate constants for RH and $RONO_2$ reacting with OH, respectively. These values were taken from the published literature (Atkinson and Arey, 2003; Simpson et al., 2003; Wang et al., 2013). J_{RONO2} is the photolysis frequency of alkyl nitrates, which was also obtained from the published literature (Bertman et al., 1995; Simpson et al., 2003; Wang et al., 2013). Details of this model can be found elsewhere (Bertman et al., 1995; Sun et al., 2018).

2.4. The MCM chemical box model

An observation-constrained chemical box model constructed based on the Master Chemical Mechanism version 3.3.1 (MCMv3.3.1; http://mcm.leeds.ac.uk/MCM/) was applied to further diagnose the formation regimes of alkyl nitrates in the YelRD region. A detailed description of this state-of-the-art chemical mechanism has been provided previously (Jenkin et al., 2003; Jenkin et al., 2015; Saunders et al., 2003).

In the present study, the MCM model was utilized to examine the sensitivity of the C_1–C_5 $RONO_2$ formation to different hydrocarbon groups. The measured VOC species were categorized into six groups, namely, parent alkanes (PA; including methane for $MeONO_2$, ethane for $EtONO_2$, propane for $1\text{-}PrONO_2$ and $2\text{-}PrONO_2$, n-butane for $2\text{-}BuONO_2$, n-pentane for $2\text{-}PeONO_2$ and $3\text{-}PeONO_2$, and i-pentane for $3\text{-}Me\text{-}2\text{-}BuONO_2$), alkanes with carbon numbers ≥4 (C4HC; except for the parent alkanes), alkenes, reactive aromatics (R-AROM; including all measured aromatics except for benzene), low-reactivity hydrocarbons (LRHC; including ethyne and benzene), and biogenic hydrocarbons (BHC; including isoprene and α/β-pinenes). Detailed information on this classification has been provided elsewhere (Sun et al., 2018; Xue et al., 2014a).

During the simulation, the model was constrained by the observed data of O_3, CO, SO_2, NO, NO_2, HONO, J_{NO2}, temperature and relative humidity, which were averaged into a time resolution of 5 min. As for hydrocarbons, they were read into the model with a time resolution of 2 h and processed as follows: the in-situ measurement data were directly used as model inputs during the daytime, and the nighttime concentrations were estimated according to the regressions with CO (for most hydrocarbons except for isoprene) and temperature (for isoprene). The model was not
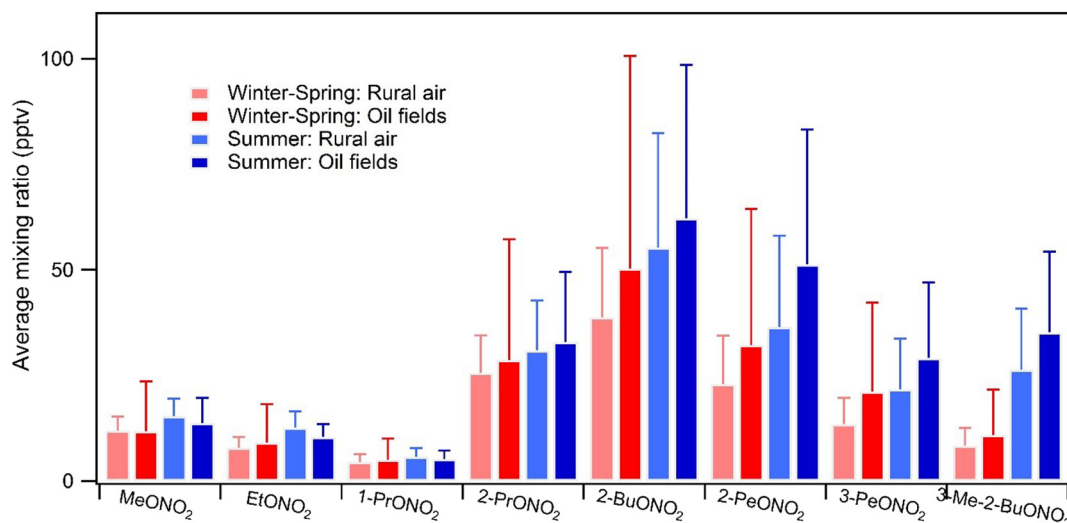

Fig. 2. Average mixing ratios of major alkyl nitrates in the ambient air and oil fields during the measurement campaigns. The error bars indicate the standard deviations of the data.

constrained with the measured $RONO_2$ data but simulated the $RONO_2$ concentrations with inputs of their precursors. A series of sensitivity simulations with 10% reductions in the concentrations of the target hydrocarbon groups were conducted to calculate the relative incremental reactivity (RIR). RIR is defined here as the ratio of percentage decrease in the maximum model-simulated $RONO_2$ concentrations to percentage reduction in the concentrations of the target hydrocarbon group. A higher positive RIR value means that the alkyl nitrate production is more sensitive to this VOC group. This model has been successfully deployed to examine the relationships of secondary pollutants such as O_3, alkyl nitrates, carbonyls, and peroxyacetyl nitrate with their precursors (Sun et al., 2018; Xue et al., 2014a; Xue et al., 2014b; Yang et al., 2018).

3. Results and discussion

3.1. General characteristics

Table 3 documents the descriptive statistics of C_1–C_5 $RONO_2$ and related species observed both at the rural site and in open oil fields. Fig. 2 shows the comparisons of the measured $RONO_2$ species in summer versus in winter-spring and between rural area and oil fields. For the rural site, the C_1–C_5 $RONO_2$ exhibited higher levels in summer (with average $\pm$ standard deviation of 204 $\pm$ 93 pptv) than in winter-spring seasons (133 $\pm$ 53 pptv). On the contrary, their precursors including C_1–C_5 hydrocarbons and NO_x showed an opposite seasonal pattern with much lower concentrations in summer than in winter-spring. All of the differences are statistically significant ($p < 0.01$). Such seasonal variations of alkyl nitrates and precursors are expected and are attributed to the more intense photochemistry in summer than in cold seasons. They demonstrate the importance of photochemical production in determining the abundance and variability of atmospheric alkyl nitrates. C_3–C_5 $RONO_2$ (except for 1-$PrONO_2$) were the most abundant species in both seasons, accounting for 82 $\pm$ 5% and 81 $\pm$ 3% of the total measured $RONO_2$ in summer and winter-spring, respectively. In comparison, $MeONO_2$, $EtONO_2$ and 1-$PrONO_2$ only composed a small fraction (10–34%) of total $RONO_2$. In summer, the C_3–C_5 species made a larger contribution to the total $RONO_2$ than in winter-spring, and in particular the proportion of 3-Me-2-$BuONO_2$ increased from 6% in winter-spring to 13% in summer. This may be due to the stronger evaporation of VOCs (mainly longer alkanes) from oil fields, and suggests more intensive photochemical formation of heavier alkyl nitrates in summer in the study region (Zheng et al., 2018). The measured C_1–C_5 $RONO_2$ species only accounted for a small fraction of NO_y (0.2–2.6% and 0.4–3.6% in winter-spring and summer, respectively), which is consistent to those observed in Beijing (0.1–3.8%; Sun et al., 2018).

Comparison of data between ambient rural area and open oil fields can reflect the influence of oil extraction on the alkyl nitrate formation. The average mixing ratios of major C_2–C_5 hydrocarbons calculated from all samples inside the oil fields were about an order of magnitude higher than those recorded at the rural site (see Table 3). This highlights the strong emissions of VOCs in the oil fields. As expected, the summed C_1–C_5 $RONO_2$ species exhibited substantially higher mixing ratios (240 $\pm$ 126 and 169 $\pm$ 119 pptv in summer and winter-spring, respectively) in the oil fields than at the rural site (204 $\pm$ 93 and 133 $\pm$ 53 pptv). An interesting result is the slightly different chemical compositions of alkyl nitrates between oil fields and the rural atmosphere. Specifically, in the open oil fields, $MeONO_2$, $EtONO_2$ and 1-$PrONO_2$ presented even slightly lower concentrations, whilst the other heavier $RONO_2$ components showed larger enhancements compared to the rural atmospheres (refer to Table 3 and Fig. 2). Correspondingly, during the whole air sampling periods, C_4–C_5 $RONO_2$ made a larger contribution of 73% in oil fields compared to 66% at the rural site. This indicates that oil field emissions may promote the production of longer-chain $RONO_2$ (Neuman et al., 2012).

Table 4 compares the ambient concentration levels of C_1–C_5 $RONO_2$ at the rural site in the Yellow River Delta region with those obtained from the other locations. Overall, the ambient mixing ratios of $RONO_2$

Table 4
Comparison of C_1–C_5 $RONO_2$ mixing ratios (mean $\pm$ stdev) in the Yellow River Delta with other previous observations. (Units: pptv unless otherwise specified; w in brackets indicates winter).

species	Rural				Coastal									Mountain	Urban	
	YelRD	YelRD (w)	CP (05)[1a]	CP (08)[1a]	Seacoast New England[2a]	Seacoast New England (w)[2b]	Karachi (w)[3]	HKUST[4a]	HKUST (w)[4b]	Tai O[5]	Tai O (w)[5]	TMS[6]	TW[6]	CRAES[1b]
$MeONO_2$	15.3 ± 4.1	11.9 ± 3.4	5.0 ± 2.7	11.6 ± 5.3	3.1 ± 1.3	3.4 ± 1.3	10.6 ± 4.1	12.0 ± 2.9	8.8 ± 1.9	17.3 ± 3.7	11.0 ± 1.2	10.9 ± 0.4	12.6 ± 0.5	12.3 ± 4.7
$EtONO_2$	12.6 ± 3.9	7.8 ± 2.5	9.5 ± 4.8	29.4 ± 17.3	3.4 ± 1.6	4.2 ± 0.8	15.5 ± 4.6	7.2 ± 4.1	9.8 ± 3.1	9.4 ± 2.4	10.6 ± 1.0	12.1 ± 0.5	13.3 ± 0.6	29.7 ± 13.9
1-$PrONO_2$	5.7 ± 2.0	4.5 ± 1.8	3.6 ± 2.3	3.6 ± 2.4	1.2 ± 0.8	1.4 ± 0.3	5.0 ± 1.6	1.8 ± 1.4	3.3 ± 1.4	2.4 ± 0.9	3.5 ± 0.5	3.8 ± 0.2	4.0 ± 0.2	3.9 ± 2.0
2-$PrONO_2$	30.8 ± 11.8	25.5 ± 8.9	23.7 ± 15.2	24.9 ± 16.5	6.5 ± 4.7	7.4 ± 1.7	21.0 ± 7.6	11.7 ± 8.3	26.1 ± 14.1	15.9 ± 5.1	23.8 ± 2.2	24.1 ± 1.1	26.3 ± 1.2	26.2 ± 14.1
2-$BuONO_2$	55.2 ± 27.2	38.7 ± 16.5	27.9 ± 21.4	40.2 ± 31.5	3.6 ± 3.1	6.5 ± 1.8	25.1 ± 12.8	13.5 ± 1.0	37.6 ± 15.0	19.7 ± 8.1	28.9 ± 3.2	32.0 ± 1.7	34.2 ± 1.9	42.5 ± 27.9
2-$PeONO_2$	36.4 ± 21.7	22.9 ± 11.6	14.3 ± 12.0	11.9 ± 9.5	2.0 ± 2.1	2.4 ± 0.8	–	–	–	5.4 ± 2.3	6.9 ± 0.7	–	–	13.5 ± 8.8
3-$PeONO_2$	21.6 ± 12.1	13.4 ± 6.3	8.9 ± 7.2	7.7 ± 5.8	1.4 ± 1.4	1.8 ± 0.5	–	–	–	4.8 ± 2.0	6.5 ± 0.6	–	–	8.2 ± 5.2
3-Me-2-$BuONO_2$	26.4 ± 14.4	8.3 ± 4.2	15.5 ± 11.9	15.5 ± 11.9	–	–	–	–	–	–	–	–	–	17.2 ± 10.7

1: (1a) June–August (summer) and (1b) January–February (winter), 2002 (Russo et al., 2010). 2: December 1998–January 1999 (Barletta et al., 2002). 3: Hong Kong University of Science and Technology (HKUST); (3a) May and August 2011 (summer) and (3b) November 2011 and February 2012 (winter) (Song et al., 2018); 4: August 2001–December 2002 (Simpson et al., 2006). 5: Changping (CP), Chinese Research Academy of Environmental Science (CRAES); (5a) June–July 2005 and July–August 2008 and (5b) July–August 2008 (Sun et al., 2018). 6: Tai Mo Shan (TMS), Tsuen Wan (TW); September–November 2010 (Ling et al., 2016).
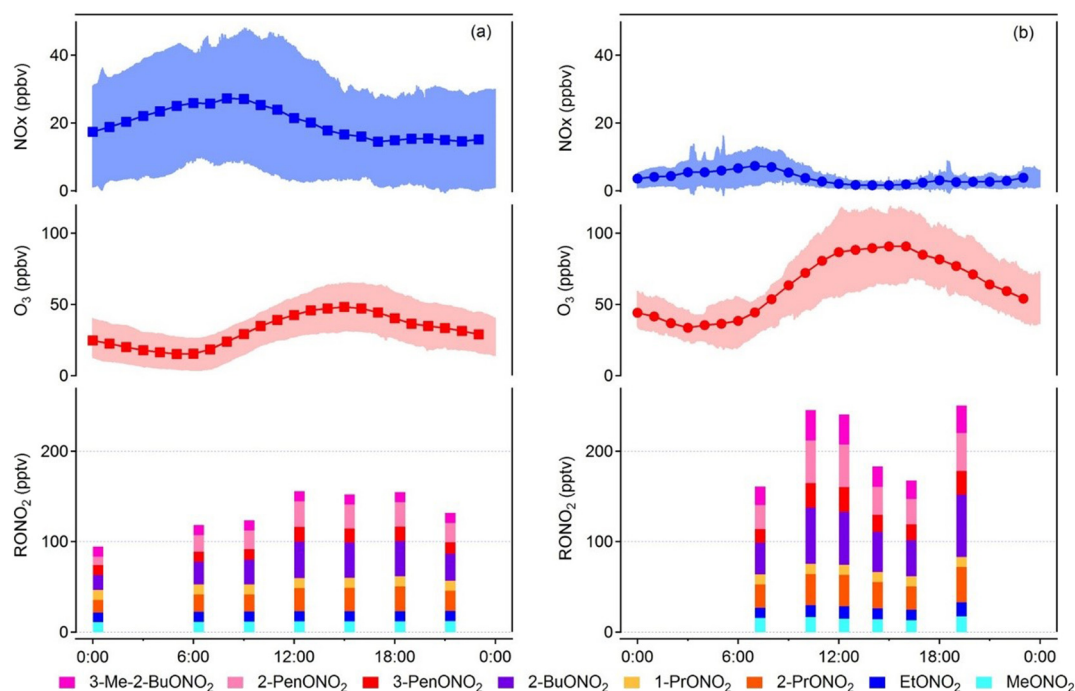
Fig. 3. Average diurnal variations of O_3, NO_x and C_1–C_5 $RONO_2$ in (a) winter-spring and (b) summer, respectively. The shaded area indicates the standard deviation of the mean.

observed in the present study are among the highest levels ever reported by the previous studies, and are even higher than those determined in the polluted areas of Beijing and Hong Kong (Ling et al., 2016; Sun et al., 2018). This elucidates the severity of alkyl nitrates and photochemical pollution in the Yellow River Delta region with complex emission sources such as oil and natural gas extraction, and the petrochemical industry. Furthermore, the chemical speciation of alkyl nitrates in the Yellow River Delta region is also slightly different from those in the other areas. The heavier C_4–C_5 $RONO_2$ species contributed to a much higher fraction compared to the other regions. For example, the average mixing ratios of C_5 $RONO_2$ species were 2–17 fold higher than those measured from the other studies. As discussed above, the higher fraction of longer-chain $RONO_2$ species should be attributed to the influence of oil field emissions in the study region. We will further examine the formation mechanisms of these most abundant longer-chain $RONO_2$ by chemical box modeling analysis in Section 3.4.

Fig. 3 presents the average diurnal variations of O_3, NO_x, and C_1–C_5 $RONO_2$ at the rural site. NO_x showed similar diurnal patterns in both seasons with a maximum in the early morning and a trough in the afternoon and early evening. O_3 displayed a well-defined diurnal profile with a broad daytime concentration peak in both summer and winter-spring seasons. In comparison, the diurnal patterns of $RONO_2$ showed some seasonal variability. During the winter-spring campaign, the C_1–C_5 $RONO_2$ showed a daytime concentration peak that tracks well with the diurnal pattern of O_3. During the summer phase, $RONO_2$ showed two concentration peaks at noon and in the early evening. The noon-time peak should be due to the in-situ photochemical production, whilst the evening peak is probably ascribed to the regional transport of aged plumes to the study site. We examined the diurnal variations case by case, and found that four of ten cases (i.e., 15th, 16th, 29th June and 9th July 2017) showed the evening concentration peaks of alkyl nitrates (and also O_3). This suggests the frequent transport of photochemically processed plumes to the rural areas in summer.

3.2. Effects of regional transport and biomass burning on alkyl nitrates

In order to assess the impact of air pollution transport on the observed alkyl nitrates, we calculated backward trajectories using the

HYSPLIT model (Draxler et al., 2018) for all of the VOC samples. Briefly, trajectories were computed for each VOC sample with the ending point at an altitude of 100 m above ground level over the study site. The meteorological archive data were provided by the Global Data Assimilation System (GDAS) (http://ready.arl.noaa.gov/archives.php). According to the sequential reaction model analysis (refer to Section 3.3 and Fig. 7), the photochemical evolution of alkyl nitrates occurred well within 4 days in winter-spring and 2 days during the summer campaign. Therefore, we computed the 4-day and 2-day backward trajectories for the winter-spring and summertime samples, respectively. These trajectories were then categorized into several major groups with the aid of a cluster analysis tool within the HYSPLIT model (Sun et al., 2016). The identified major types of air masses and their chemical speciation of alkyl nitrates are presented in Fig. 4.

During the winter-spring measurement period, the air masses corresponding to the $RONO_2$ observations can be segregated into two types according to their origins and transport trajectories. One came from the northwest passing over Mongolia and North China at higher altitudes (referred to as Type "NW"), and the other came from the southwest travelling over the central and southern parts of the polluted North China Plain at low speeds (referred to as Type "SW"). Under the control of the Mongolia-Siberian high pressure in winter-spring, the air mass Type "NW" occurred more frequently with a fraction of 58%, and Type "SW" contributed to the remaining 42%. As shown in Fig. 4c, the "SW" air masses contained much higher levels of alkyl nitrates compared to "NW" ($p < 0.05$). This is consistent with the facts that the "SW" air parcels had passed over the highly polluted North China Plain region and that a number of oil fields and petrochemical plants are located to the southwest of the study site.

In summer, three types of air masses were classified. Type "SW-local" refers to the air masses coming from the southwest/west sectors and travelling at very low speeds; Type "SW-regional" also comes from the southwest sector but travelling at relatively faster speeds; and Type "SE" represents the air masses originating from the ocean and coming from the southeast sector. All of these three types of air masses had passed over the densely populated areas in eastern China. During the measurement campaign, the Type "SW-local" occurred the most frequently with a fraction of 41%, followed
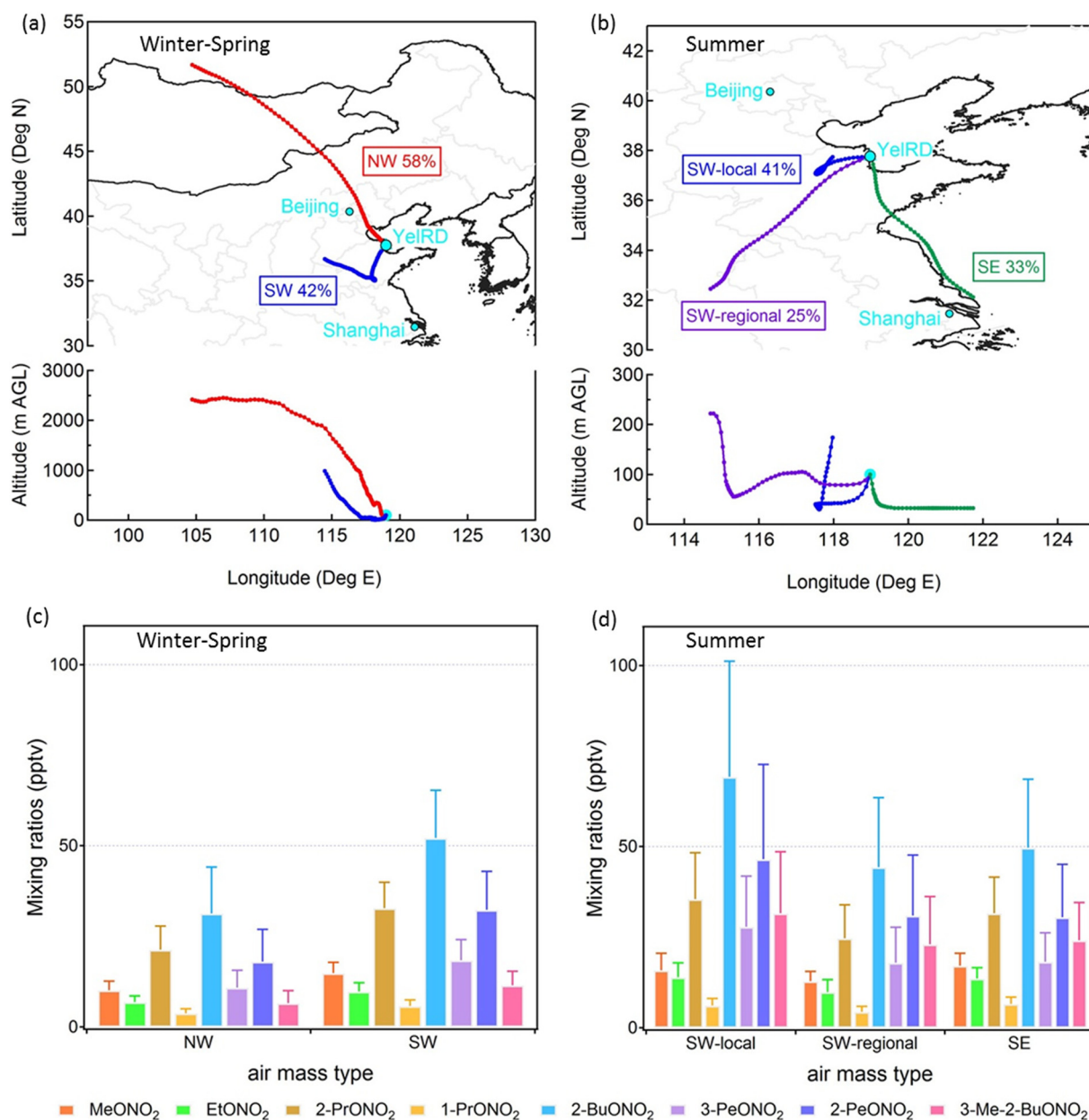
Fig. 4. The upper panels (a) and (b) show the major air mass types and the 4-day backward trajectories in winter-spring (2-day backward trajectories in summer) arriving at the sampling site; the lower panels (c) and (d) indicates the distributions of C_1–C_5 $RONO_2$ in different types of air masses. Error bars stand for the standard deviations of the measurement data.

by Type "SE" (33%) and "SW-regional" (25%). Fig. 4d shows that the abundances of most $RONO_2$ species were the highest in the air mass Type "SW-local", whilst those in the air masses of "SW-regional" and "SE" were comparable. An exception is $MeONO_2$ that showed the highest concentrations in the sea-originating "SE" air masses ($p < 0.05$). This suggests the influence of marine emissions on the observed $MeONO_2$ at our study site.

Overall, the above analyses indicate that the observed alkyl nitrate pollution was affected by the regional transport of polluted air masses from the southwest sectors. Especially, the slowly-moving air masses that had passed over the oil fields and petrochemical plants contained the highest levels of alkyl nitrates (and also their parent hydrocarbons). Besides, marine emissions made a considerable contribution to the enhancement of $MeONO_2$.

Furthermore, it was also found that the observed photochemical pollution (including alkyl nitrates) in the YelRD region was significantly affected by biomass burning. Early- to mid-June is the harvest season of winter wheat in the North China Plain, during which the regional air quality can be substantially deteriorated by open burning of wheat straw (Chen et al., 2017; and references therein). Indeed, examination of the daily fire maps illustrates the frequent regional burning of biomass in northern China during 7–21 June 2017 (https://earthdata.nasa.gov/earth-observation-data/near-real-time/firms). Fig. 5 presents the time series of major air pollutants observed on 8 June, a typical case with influence of biomass burning. In the early morning (e.g., 7:00–8:00 LT), elevated concentrations of NO_x, NO_y and CO were observed at the study site with dominance of southwesterly winds. After that, the ambient concentrations of secondary pollutants such as O_3 and $RONO_2$ sharply increased, with the maximum concentrations of 148 ppbv and 559 pptv being recorded at around 10:30 AM. Such a diurnal variation pattern is different from the usual ones with afternoon peaks of O_3 and $RONO_2$, and the significant increases in O_3 (~100 ppbv) and $RONO_2$ (~275 pptv) in the early morning period (i.e., 7:00–10:30 LT) suggest the transport of polluted and well-processed plumes in addition to the in-situ
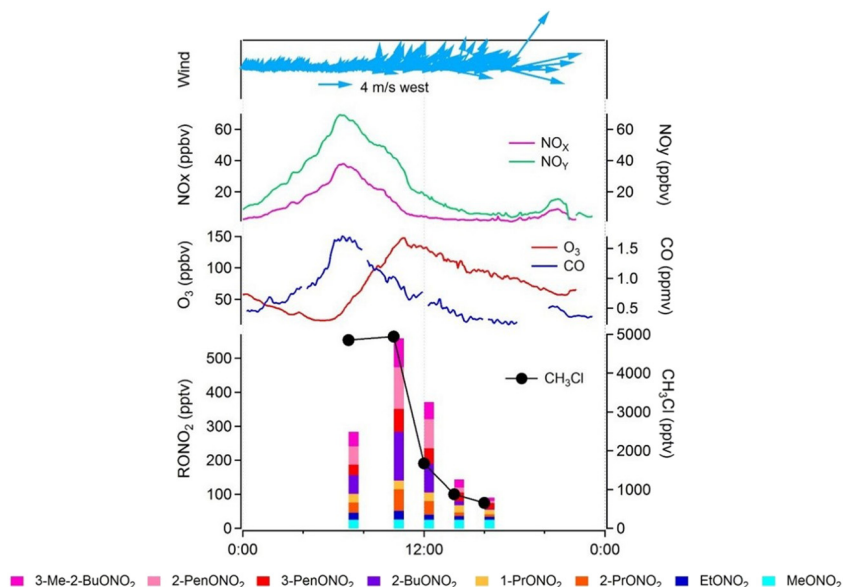
Fig. 5. Time series of trace gases and meteorological parameters observed on 8 June 2017.

photochemical formation. Methyl chloride (CH_3Cl), a tracer for biomass burning emissions (Crutzen et al., 1979; Simpson et al., 2002), showed very high concentrations (~4850 pptv) in the early morning period, which coincides with the elevated concentrations of primary pollutants and the significant increases in O_3 and $RONO_2$. Similar diurnal profiles were also found for some other combustion tracers such as ethyne and

Fig. 6. Fire map (https://earthdata.nasa.gov/earth-observation-data/near-real-time/firms) showing the daily fire spots over eastern China together with 2-day backward trajectories on 8 June 2017.

benzene (figures not shown). Two-day backward trajectories clearly showed that the air masses came from the southwest sectors with intense fire spots (see Fig. 6). This confirms the effects of biomass burning on the observed O_3 and $RONO_2$ pollution. Pollution events with influence of biomass burning were also observed on 9, 16, and 18 June, indicating that biomass burning is an important emission source in the YelRD region in June.

3.3. Photochemical evolution of alkyl nitrates

The simplified sequential reaction model, as described in Section 2.3, was used to examine the photochemical evolution of $RONO_2$ and their parent alkanes, and meanwhile to estimate the photochemical age of air masses. Comparison of the observed $RONO_2$/RH ratios versus the model predicted photochemical curves can provide some insights into the sources of alkyl nitrates. If the observed ratios lie on the predicted photochemical curve, it is believed that the oxidation of parent alkanes is the predominant source of the target $RONO_2$ species, otherwise observed ratios higher than photochemical curve suggests the existence of additional source of $RONO_2$ besides the oxidation of parent alkanes (Bertman et al., 1995). In the present study, [2-$BuONO_2$]/[n-butane] was selected as the independent ratio, considering that 2-$BuONO_2$ was the most abundant $RONO_2$ species and is chiefly formed from the photochemical oxidation of n-butane (Bertman et al., 1995; Reeves et al., 2007; Sun et al., 2018). All of the samples were classified into three categories: summer oil fields (SO), summer ambient air (SA), and winter ambient air (WA), according to the sampling periods and locations.

Fig. 7 shows the scatter plots of the observed individual C_1–C_5 [$RONO_2$]/[RH] versus [2-$BuONO_2$]/[n-butane] and the comparisons with the model predicted photochemical curves. The photochemical age of air masses shows clear temporal and spatial variabilities. The air masses sampled in the open oil fields were quite fresh with their estimated photochemical ages generally shorter than half day. In comparison, the air masses encountered at rural study site were more aged, with photochemical ages of up to two days in summer and four days in the winter-spring seasons. Furthermore, from a diurnal variation perspective, the air masses in the afternoon and evening were more photochemically processed than those in the morning. The above tempo-spatial variations were as expected because the air masses had undergone photochemical processing before arriving at the rural areas and alkyl nitrates have a longer lifetime in winter-spring than in summer.
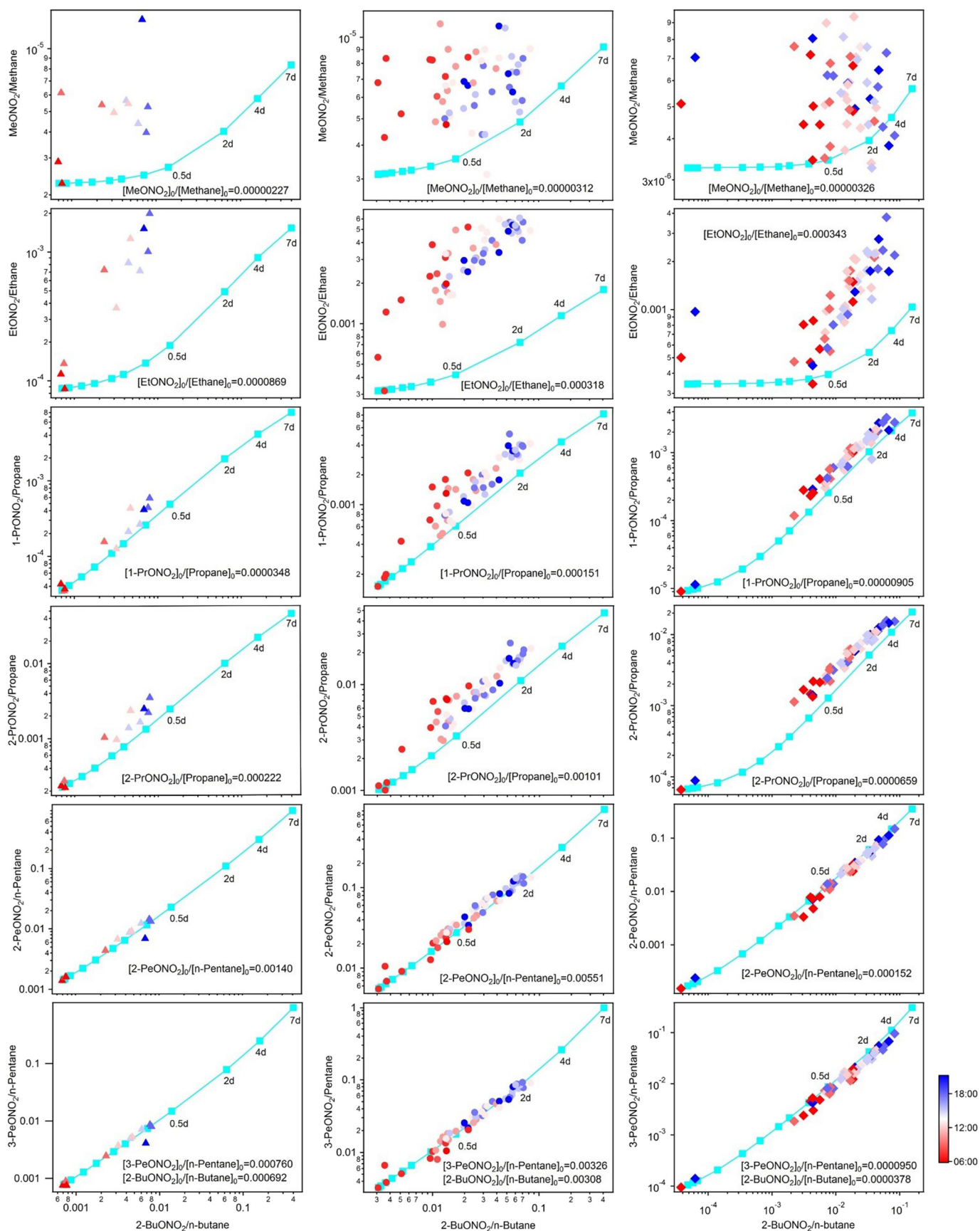
Fig. 7. Relationships between C_1–C_5 $RONO_2$/RH and 2-BuONO$_2$/n-butane. The rainbow triangles, circles and rhombuses represent the observed ratios of summer oil fields, summer rural air and winter rural air, respectively. The blue lines with squares are the theoretical photochemical curves. $[RONO_2]_0/[RH]_0$ was calculated as the initial background ratio values (the observed lowest ratio).

As to the RONO$_2$ sources, similar results were found both at oil fields and at the rural site. Specifically, the observed values of C$_3$-C$_5$ [RONO$_2$]/[RH] agreed very well with the theoretical photochemical curves, confirming that the C$_3$–C$_5$ RONO$_2$ species were mainly produced from the photochemical oxidation of direct parent alkanes, i.e., propane, *n*-butane and *n*-pentane. This result was consistent with the conclusion of previous studies that the sources of longer-chain RONO$_2$ species were dominated by the oxidation of parent hydrocarbons (Russo et al., 2010; Sun et al., 2018). A few measured C$_5$ [RONO$_2$]/[RH] ratios were under the modelled curves, which may be explained by fragmentation of *n*-pentane to form shorter-chain RO$_2$ radical (Reeves et al., 2007). In contrast, the measured C$_1$–C$_2$ [RONO$_2$]/[RH] ratios lay above the theoretical photochemical curves to varying degrees, indicating the existence of additional sources other than photochemical oxidation of methane and ethane. As discussed above, marine emissions and biomass burning may be important sources of RONO$_2$ species, particularly MeONO$_2$ in the case of marine emissions. Another possible source of C$_1$–C$_2$ RONO$_2$ is the degradation of longer-chain hydrocarbons other than the parent alkanes (Zeng et al., 2018).

3.4. Relationships of RONO$_2$ with precursors

To better elucidate the formation mechanisms of alkyl nitrates in the YelRD region and in open oil fields, we have examined the detailed relationships between the observed RONO$_2$ species and their major precursors. RIR was calculated by the observation-based MCM model for the major hydrocarbon groups, namely, PA, C4HC, alkenes, R-AROM, LRHC and BHC (see details in Section 2.4). Considering that the concentrations of MeONO$_2$, EtONO$_2$ and 1-PrONO$_2$ were very low (see Fig. 2), here we focused on the formation mechanisms of the other abundant C$_3$–C$_5$ RONO$_2$ compounds. Modeling analyses were conducted for a photochemical pollution episode observed on 9 July 2017, when concurrent observations of RONO$_2$ and their precursors were made both at the rural site and in the open oil fields. All major hydrocarbon groups presented positive RIR values, implying the important role of VOCs in the RONO$_2$ formation (Lyu et al., 2017).

Fig. 8a shows the model-calculated RIR values of the major hydrocarbon groups for the individual RONO$_2$ species at the rural study site. Clearly, parent hydrocarbons (i.e., propane for 2-PrONO$_2$, *n*-butane for 2-BuONO$_2$, *n*-pentane for 2-PeONO$_2$ and 3-PeONO$_2$, and *i*-pentane for 3-Me-2-BuONO$_2$) showed the highest positive RIR values, demonstrating their overwhelming contributions to the formation of alkyl nitrates. This was consistent with the results obtained from the above-mentioned photochemical curve analyses.

The RIR values obtained from the open oil fields are documented in Fig. 8b. Similarly, PA shows the highest positive RIR values for all of the C$_3$–C$_5$ RONO$_2$ species, indicating the predominant role of oxidation of parent alkanes in the photochemical formation of alkyl nitrates. This agrees well with the results derived from the sequential reaction model as described in Section 3.3. Moreover, longer-chain alkanes (i.e., C4HC) also showed modest positive RIR values for all of these RONO$_2$ species, suggesting their contributions to the RONO$_2$ formation in the open oil fields. It is already known that longer-chain alkanes, cycloalkanes and aromatics are the principal VOC compounds emitted from oil fields (Gilman et al., 2013; Zheng et al., 2018). Therefore, the abundant emissions of longer-chain alkanes from oil extraction and evaporation and the subsequent photochemical oxidation may explain the observed much higher C$_3$–C$_5$ alkyl nitrates in the oil fields (see Section 3.1).

4. Summary

Intensive measurements of C$_1$–C$_5$ RONO$_2$ and related parameters were carried out at a rural site and in open oil fields of the Yellow River Delta region during February–April and June–July of 2017. Alkyl nitrates showed higher mixing ratios in summer than in winter-
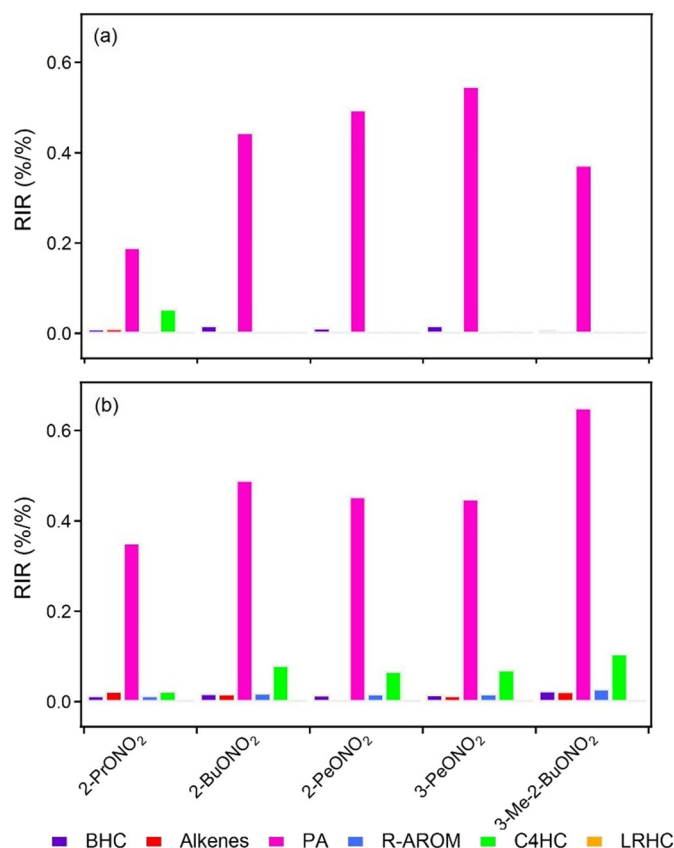

Fig. 8. The OBM-calculated daytime average RIR for major precursor groups of C$_3$–C$_5$ RONO$_2$ (a) at the rural site and (b) in open oil fields in summer.

spring, which is opposite to the seasonal pattern of their parent hydrocarbons. Enhanced levels of heavier C$_3$–C$_5$ RONO$_2$ compounds were observed in the oil fields compared to the rural atmosphere. In-situ photochemical production and regional transport are two major processes contributing to the observed alkyl nitrate pollution. The alkyl nitrates and photochemical pollution in the YelRD region were significantly affected by the oil field emissions and biomass burning, and ocean emissions were an important source of methyl nitrate. Oxidation of parent alkanes is the dominant source of C$_3$–C$_5$ RONO$_2$ in the YelRD region, whilst longer-chain alkanes with >4 carbon atoms were important precursors of alkyl nitrates in the oil fields. This study elucidates the serious alkyl nitrate pollution and the complex emission sources in the YelRD region, where such kind of previous studies were scarce in this region.

References

Arey, J., Aschmann, S.M., Kwok, E.S.C., Atkinson, R., 2001. Alkyl nitrate, hydroxyalkyl nitrate, and hydroxycarbonyl formation from the NO$_x$-air photooxidations of C$_5$–C$_8$ n-alkanes. J. Phys. Chem. 105, 1020–1027.

Atkinson, R., Arey, J., 2003. Atmospheric degradation of volatile organic compounds. Chem. Rev. 103, 4605–4638.

Atkinson, R., Baulch, D.L., Cox, R.A., Crowley, J.N., Hampson, R.F., Hynes, R.G., Jenkin, M.E., Rossi, M.J., Troe, J., 2006. Evaluated kinetic and photochemical data for atmospheric chemistry: volume II-gas phase reactions of organic species. Atmos. Chem. Phys. 6, 3625–4055.

Atlas, E., Pollock, W., Greenberg, J., Heidt, L., Thompson, A.M., 1993. Alkyl nitrates, nonmethane hydrocarbons, and halocarbon gases over the equatorial Pacific Ocean during SAGA 3. J. Geophys. Res. Atmos. 98, 16933–16947.

Barletta, B., Meinardi, S., Simpson, I.J., Khwaja, H.A., Blake, D.R., Rowland, F.S., 2002. Mixing ratios of volatile organic compounds (VOCs) in the atmosphere of Karachi, Pakistan. Atmos. Environ. 36, 3429–3443.

Bertman, S.B., Roberts, J.M., Parrish, D.D., Buhr, M.P., Goldan, P.D., Kuster, W.C., Fehsenfeld, F.C., 1995. Evolution of alkyl nitrates with air mass age. J. Geophys. Res. Atmos. 100, 22805–22813.

Blake, N.J., Blake, D.R., Swanson, A.L., Atlas, E., Flocke, F., Rowland, F.S., 2003. Latitudinal, vertical, and seasonal variations of C_1–C_4 alkyl nitrates in the troposphere over the Pacific Ocean during PEM-Tropics A and B: Oceanic and continental sources. J. Geophys. Res. Atmos. 108, 171–181.

Chen, J.M., Li, C.L., Ristovski, Z., Milic, A., Gu, Y.T., Islam, M.S., Wang, S.X., Hao, J.M., Zhang, H.F., He, C.R., Guo, H., Fu, H.B., Miljevic, B., Morawska, L., Thai, P., Lam, Y.F., Pereira, G., Ding, A.J., Huang, X., Dumka, U.C., 2017. A review of biomass burning: emissions and impacts on air quality, health and climate in China. Sci. Total Environ. 579, 1000–1034.

Colman, J.J., Swanson, A.L., Meinardi, S., Sive, B.C., Blake, D.R., Rowland, F.S., 2001. Description of the analysis of a wide range of volatile organic compounds in whole air samples collected during PEM-Tropics A and B. Anal. Chem. 73, 3723–3731.

Crutzen, P.J., Heidt, L.E., Krasnec, J.P., Pollock, W.H., W., S., 1979. Biomass burning as a source of atmospheric gases CO, H_2, N_2O, NO, CH_3Cl, and COS. Nature 282, 253–256.

Day, D.A., Dillon, M.B., Wooldridge, P.J., Thornton, J.A., Rosen, R.S., Wood, E.C., C., C.R., 2003. On alkyl nitrates, O_3, and the "missing NO_y". J. Geophys. Res. Atmos. 108, 4501.

Draxler, R., Stunder, B., Rolph, G., Stein, A., Taylor, A., 2018. HYSPLIT4 USER'S GUIDE Version 4 - Last Revision: February 2018. Retrieved from. https://www.arl.noaa.gov/documents/reports/hysplit_user_guide.pdf.

Gilman, J.B., Lerner, B.M., Kuster, W.C., de Gouw, J.A., 2013. Source signature of volatile organic compounds from oil and natural gas operations in northeastern Colorado. Environ. Sci. Technol. 47, 1297–1305.

Jenkin, M.E., Clemitshaw, K.C., 2000. Ozone and other secondary photochemical pollutants: chemical processes governing their formation in the planetary boundary layer. Atmos. Environ. 34, 2499–2527.

Jenkin, M.E., Saunders, S.M., Wagner, V., Pilling, M.J., 2003. Protocol for the development of the master chemical mechanism, MCM v3 (part B): tropospheric degradation of aromatic volatile organic compounds. Atmos. Chem. Phys. 3, 181–193.

Jenkin, M.E., Young, J.C., Rickard, A., 2015. The MCM v3.3.1 degradation scheme for isoprene. Atmos. Chem. Phys. 15, 11433–11459.

Kwok, E.S.C., Atkinson, R., 1995. Estimation of hydroxyl radical reaction rate constants for gas-phase organic compounds using a structure-reactivity relationship: an update. Atmos. Environ. 29.

Li, M., Zhang, Q., Kurokawa, J., Woo, J., He, K.B., Lu, Z.F., Ohara, T., Song, Y., Streets, D.G., Carmichael, G.R., Cheng, Y.F., Hong, C.P., Huo, H., Jiang, X.J., Kang, S.C., Liu, F., Su, H., Zheng, B., 2017. MIX: a mosaic Asian anthropogenic emission inventory under the international collaboration framework of the MICS-Asia and HTAP. Atmos. Chem. Phys. 17, 935–963.

Li, D.D., Xue, L.K., Wen, L., Wang, X.F., Chen, T.S., Mellouki, A., Chen, J.M., Wang, W.X., 2018. Characteristics and sources of nitrous acid in an urban atmosphere of northern China: results from 1-yr continuous observations. Atmos. Environ. 182, 296–306.

Ling, Z.H., Guo, H., Simpson, I.J., Saunders, S.M., Lam, S.H.M., Lyu, X.P., Blake, D.R., 2016. New insight into the spatiotemporal variability and source apportionments of C_1–C_4 alkyl nitrates in Hong Kong. Atmos. Chem. Phys. 16, 8141–8156.

Lyu, X.P., Ling, Z.H., Guo, H., Saunders, S.M., Lam, S.H.M., Wang, N., Wang, Y., Liu, M., Wang, T., 2015. Re-examination of C_1–C_5 alkyl nitrates in Hong Kong using an observation-based model. Atmos. Environ. 120, 28–37.

Lyu, X.P., Guo, H., Lam, H.M., Meinardi, S., Wang, N., Simpson, I.J., Blake, D.R., 2017. Modeling C_1–C_4 alkyl nitrate photochemistry and their impacts on O_3 production in urban and suburban environments of Hong Kong. J. Geophys. Res. Atmos. 122, 539–556.

Neuman, J.A., Aikin, K.C., Atlas, E.L., Blake, D.R., Holloway, J.S., Meinardi, S., Nowak, J.B., Parrish, D.D., Peischl, J., Perring, A.E., Pollack, I.B., Roberts, J.M., Ryerson, T.B., Trainer, M., 2012. Ozone and alkyl nitrate formation from the Deepwater Horizon oil spill atmospheric emissions. J. Geophys. Res. Atmos. 117.

Reeves, C.E., Slemr, J., Oram, D.E., Worton, D.R., Penkett, S.A., Stewart, D.J., Purvis, R., Watson, N., Hopkins, J., Lewis, A., Methven, J., Blake, D.R., Atlas, E., 2007. Alkyl nitrates

in outflow from North America over the North Atlantic during Intercontinental Transport of Ozone and Precursors 2004. J. Geophys. Res. Atmos. 112, 409–427.

Russo, R.S., Zhou, Y., Haase, K.B., Wingenter, O.W., Frinak, E.K., Mao, H., Talbot, R.W., Sive, B.C., 2010. Temporal variability, sources, and sinks of C_1–C_5 alkyl nitrates in coastal New England. Atmos. Chem. Phys. 10, 1865–1883.

Saunders, S.M., Jenkin, M.E., Derwent, R.G., Pilling, M.J., 2003. Protocol for the development of the Master Chemical Mechanism, MCMv3 (part A): tropospheric degradation of non-aromatic volatile organic compounds. Atmos. Chem. Phys. 3, 161–180.

Simpson, I.J., Meinardi, S., Blake, D.R., Blake, N.J., Rowland, F.S., Atlas, E., Flocke, F., 2002. A biomass burning source of C_1–C_4 alkyl nitrates. Geophys. Res. Lett. 29 (21-21-21-24).

Simpson, I.J., Blake, N.J., Blake, D.R., Atlas, E., Flocke, F., Crawford, J.H., Fuelberg, H.E., Kiley, C.M., Meinardi, S., Rowland, F.S., 2003. Photochemical production and evolution of selected C_2–C_5 alkyl nitrates in tropospheric air influenced by Asian outflow. J. Geophys. Res. Atmos. 108, 8808.

Simpson, I.J., Wang, T., Guo, H., Kwok, Y., Flocke, F., Atlas, E., Meinardi, S., Rowland, F.S., Blake, D.R., 2006. Long-term atmospheric measurements of C_1–C_5 alkyl nitrates in the Pearl River Delta region of southeast China. Atmos. Environ. 40, 1619–1632.

Sommariva, R., Trainer, M., de Gouw, J.A., Roberts, J.M., Warneke, C., Atlas, E., Flocke, F., Goldan, P.D., Kuster, W.C., Swanson, A.L., Fehsenfeld, F.C., 2008. A study of organic nitrates formation in an urban plume using a Master Chemical Mechanism. Atmos. Environ. 42, 5771–5786.

Song, J., Zhang, Y., Huang, Y., Ho, K.F., Yuan, Z., Ling, Z., Niu, X., Gao, Y., Cui, L., Louie, P.K.K., Lee, S.C., Lai, S., 2018. Seasonal variations of C_1–C_4 alkyl nitrates at a coastal site in Hong Kong: influence of photochemical formation and oceanic emissions. Chemosphere 194, 275–284.

Sun, L., Xue, L.K., Wang, T., Gao, J., Ding, A.J., Cooper, O.R., Lin, M.Y., Xu, P.J., Wang, Z., Wang, X.F., Wen, L., Zhu, Y.H., Chen, T.S., Yang, L.X., Wang, Y., Chen, J.M., Wang, W.X., 2016. Significant increase of summertime ozone at Mount Tai in Central Eastern China. Atmos. Chem. Phys. 16, 10637–10650.

Sun, J.J., Li, Z.Y., Xue, L.K., Wang, T., Wang, X.F., Gao, J., Nie, W., Simpson, I.J., Gao, R., Blake, D.R., Chai, F.H., Wang, W.X., 2018. Summertime C_1–C_5 alkyl nitrates over Beijing, northern China: spatial distribution, regional transport, and formation mechanisms. Atmos. Res. 204, 102–109.

Wang, T., Ding, A.J., Gao, J., Wu, W.S., 2006. Strong ozone production in urban plumes from Beijing, China. Geophys. Res. Lett. 33.

Wang, M., Shao, M., Chen, W.T., Lu, S.H., Wang, C., Huang, D.K., Yuan, B., Zeng, L.M., Zhao, Y., 2013. Measurements of C_1–C_4 alkyl nitrates and their relationships with carbonyl compounds and O_3 in Chinese cities. Atmos. Environ. 81, 389–398.

Wang, T., Xue, L.K., Brimblecombe, P., Lam, Y.F., Li, L., Zhang, L., 2017. Ozone pollution in China: a review of concentrations, meteorological influences, chemical precursors, and effects. Sci. Total Environ. 575, 1582–1596.

Worton, D.R., Reeves, C.E., Penkett, S.A., Sturges, W.T., Slemr, J., Oram, D.E., Bandy, B.J., Bloss, W.J., Carslaw, N., Davey, J., Emmerson, K.M., Gravestock, T.J., Hamilton, J.F., Heard, D.E., Hopkins, J.R., Hulse, A., Ingram, T., Jacob, M.J., Lee, J.D., Leigh, R.J., Lewis, A.C., Monks, P.S., Smith, S.C., 2010. Alkyl nitrate photochemistry during the tropospheric organic chemistry experiment. Atmos. Environ. 44, 773–785.

Xue, L.K., Wang, T., Zhang, J.M., Zhang, X.C., Deliger, Poon, C.N., Ding, A.J., Zhou, X.H., Wu, W.S., Tang, J., Zhang, Q.Z., Wang, W.X., 2011. Source of surface ozone and reactive nitrogen speciation at Mount Waliguan in western China: new insights from the 2006 summer study. J. Geophys. Res. Atmos. 116.

Xue, L.K., Wang, T., Gao, J., Ding, A.J., Zhou, X.H., Blake, D.R., Wang, X.F., Saunders, S.M., Fan, S.J., Zuo, H.C., Zhang, Q.Z., Wang, W.X., 2014a. Ground-level ozone in four Chinese cities: precursors, regional transport and heterogeneous processes. Atmos. Chem. Phys. 14, 13175–13188.

Xue, L.K., Wang, T., Wang, X.F., Blake, D.R., Gao, J., Nie, W., Gao, R., Gao, X.M., Xu, Z., Ding, A.J., Huang, Y., Lee, S.C., Chen, Y.Z., Wang, S.L., Chai, F.H., Zhang, Q.Z., Wang, W.X., 2014b. On the use of an explicit chemical mechanism to dissect peroxy acetyl nitrate formation. Environ. Pollut. 195, 39–47.

Yang, X., Xue, L.K., Wang, T., Wang, X.F., Gao, J., Lee, S.C., Blake, D.R., Chai, F.H., Wang, W.X., 2018. Observations and explicit modeling of summertime carbonyl formation in Beijing: identification of key precursor species and their impact on atmospheric oxidation chemistry. J. Geophys. Res. Atmos. 123, 1426–1440.

Zeng, L., Lyu, X., Guo, H., Zou, S., Ling, Z., 2018. Photochemical formation of C_1–C_5 alkyl nitrates in suburban Hong Kong and over the South China Sea. Environ. Sci. Technol. 52, 5581–5589.

Zheng, H., Kong, S.F., Xing, X.L., Mao, Y., Hu, T.P., Ding, Y., Li, G., Liu, D.T., Li, S.L., Qi, S.H., 2018. Monitoring of volatile organic compounds (VOCs) from an oil and gas station in northwest China for 1 year. Atmos. Chem. Phys. 18, 4567–4595.